Charge-exchange mechanisms at the threshold for inelasticity in Ne^+ collisions with surfaces

M. J. Gordon, J. Mace, and K. P. Giapis*
Division of Chemistry and Chemical Engineering, California Institute of Technology, Pasadena, California 91125, USA
(Received 24 February 2005; revised manuscript received 26 April 2005; published 28 July 2005)

We present a study on scattering of 100–1400 eV Ne^+ ions off Mg, Al, Si, and P surfaces. Exit energy distributions and yields of single-scattered Ne^+ and Ne^{2+} were separately measured to investigate charge exchange mechanisms occurring at the onset of inelastic losses in binary hard collision events. At low incident energies, collisions appear elastic and projectile ion survival is dominated by nonlocal Auger-type neutralization involving the target valence band. However, once a critical R_{min} (distance of closest approach) is reached, three phenomena occur simultaneously: Ne^{2+} generation, reversal of the Ne^+ yield trend, and inelastic losses in Ne^+ and Ne^{2+}. R_{min} values for the Ne^{2+} turn-on agree very well with the *L*-shell overlap distances of the colliding partners, suggesting that electron transfer involving the highly promoted $4f\sigma$ molecular orbital (correlated to the Ne $2p$) at close internuclear distance ($\sim$0.5 Å) is responsible. For the Ne^+ yield, a clear transition from nonlocal neutralization to R_{min}-dependent collision induced neutralization was observed. Binary collision inelasticities (Q_{bin}) were evaluated for Ne^+ and Ne^{2+} off Al and Si by taking into account electron straggling. Saturation-like behavior at $R_{min}<0.5$ Å was seen for Ne^+ ($Q_{bin}\sim$40–45 eV) and Ne^{2+} (68–75 eV). These losses fit well with double promotion of $Ne^0 \rightarrow Ne^{**}$ ($2p^4 3s^2$, 41–45 eV) and $Ne^+ \rightarrow Ne^{+**}$ ($2p^3 3s^2/3s3p$, 69–72 eV), followed by autoionization as the projectile leaves the surface region to give Ne^+ and Ne^{2+}. In contrast, Q_{bin} values for Ne^{2+} at the +2 turn-on were seen much lower (35–40 eV off Al, 55–60 eV off Si) than that required for double promotion—eliminating the possibility that Ne^{2+} is only generated in double excitation of surviving Ne^+. Thus single-electron excitation appears to be more important in the threshold region compared to the two-electron events seen at higher collision energies. In addition, the Ne^+—P system shows striking similarities with the other target cases from the perspective of a well-defined Ne^{2+} turn-on, continually increasing Ne^{2+} yield with impact energy, and inelasticity values which point to the same $4f\sigma$ excitation pathway. The decreasing R_{min} requirement for higher target *Z* in terms of Ne^{2+} production has been confirmed for the Mg through P series, where hard collision excitation is governed by *L*-shell orbital overlaps.

DOI: 10.1103/PhysRevA.72.012904 PACS number(s): 79.20.Rf, 34.70.+e, 34.50.Fa

I. INTRODUCTION

Low energy ion scattering ($E_0<5$ keV) is often used as a diagnostic tool to measure the composition and structure of the topmost atomic layers of a target surface. In this technique, the surface atomic structure (atom type, density, orientation) can be determined from the kinetic energy, intensity, and exit angle (scattering angle) of projectiles deflected by target atoms in single-scatter (SS) type events [1]. Collision processes are usually assumed to be elastic [2] while the charge state of the scattered projectile is largely governed by long-range resonant or Auger transfer of electrons from the target as a whole (nonlocal neutralization [2,3]). However, inelastic processes can occur where the kinetic energy of the incoming ion is converted into electronic excitation or ionization of the atoms in the colliding pair [2]. Inelastic effects can manifest themselves through characteristic electron or photon release from excited state decay [4,5], change in the scattered particle charge state [6–8], or shifts in the exit energy of scattered projectiles from their expected (elastic) positions [9–12]. For example, there is a long history of electron spectroscopy (ES) work on Ne^+ collisions with Na/Mg/Al/Si surfaces at keV energies relating to autoionization decay of Ne^{**} ($2p^4 3s^2$) [13–20]. In these studies, Auger emission from Ne^{**} exiting the surface is used as an after-the-fact fingerprint of electron transfer that occurs in the hard collision step at small approach distances ($R_{min}<0.5$ Å). Specifically, electrons can be transferred from the strongly promoted $4f\sigma$ molecular orbital (MO) (correlated to the Ne $2p_z$) to higher lying states at energy level "pseudocrossings" (Barat-Fano-Lichten MO theory [21]), leaving the projectile in an excited state as the collision partners recede. The overall process is thought to occur after Ne^+ is Auger neutralized (AN) on the approach to the surface, as follows [17]:

$$Ne^+(2p^5) \rightarrow Ne^0(2p^6) \rightarrow Ne^{**}(2p^4 3s^2\ {}^1D), \quad \text{AN followed by double promotion}, \tag{1}$$

$$Ne^{**}(2p^4 3s^2\ {}^1D) \rightarrow Ne^{**}(2p^4 3s^2\ {}^3P), \quad \text{core level rearrangement to populate } {}^3P, \tag{2}$$

$$Ne^{**}(2p^4 3s^2\ {}^3P \text{ or } {}^3D) \rightarrow Ne^+(2p^5) + \text{Auger release}, \quad \text{autoionization after leaving surface}. \tag{3}$$

*Corresponding author.

Unlike gas-phase collisions see ([22–24]) which almost exclusively yield the $Ne^{**}\ ^1D$ state, surface scattering results in strong ^3P production. These rearrangement mechanisms have been discussed elsewhere [14,17,25]. It has also been shown that the Auger signal from Ne^{**} decay and Ne^+ charge fraction $[I/(I+N)]$ are rather insensitive to the incoming projectile charge state (Ne^0 vs Ne^+) [16,26]—indicating that much of the Ne^+ is neutralized on the incoming path. Resonant neutralization (RN) to the Ne $3s$ on the outgoing path has been also demonstrated by VUV spectroscopy during Ne^+ bombardment of Mg/Al (15 keV, 10° incidence) [17]. In these experiments, decay emission from $Ne^*(2p^5 3s \rightarrow 2p^6)$, $Ne^{2+*}(2p^4 3s\ ^3P/^1D \rightarrow 2p^5, 2s2p^6 \rightarrow 2p^5)$, and $Ne^{2+*}(2s2p^5 \rightarrow 2p^4)$ have all been detected. The latter decay sequences involving the $2s$ hole are certainly more favorable at high collision energy, but significant RN involving the Ne $3s$ is nonetheless observed.

While ES measurements have contributed significantly to understanding gas-surface collisions, they are inherently indirect, insofar as the collision history of the projectile is totally unknown, i.e., the sequence of events, which initially generated the excited state *precursor* (seen by an Auger decay signal), cannot be extracted. Whether these excited states result from single or multiple collision events and how electron transfers in the hard collision step versus the exit trajectory affect the scattering outcome cannot be inferred from ES. Indeed, the exit state of the projectile is strongly influenced by transitions *after* the hard collision step (i.e., Ne^{**} decay yield depends strongly on the exit trajectory path [16]).

Given the limitations of ES measurements, another technique has been employed to study hard collision excitation: charge state and energy loss spectroscopy of ions leaving the surface. For instance, high ion yields (i.e., >50% Ne^+ off Mg) [27–29], multiply charged scattered projectiles (Ne^{2+} and Ne^{3+} off Mg, Al, and Si [26,30–33]), and inelastic losses (Mg, Al, and Si [29,32–34]) have been seen for single collisions involving Ne^+ at keV impact energies. In fact, single-scatter (SS) events offer a unique window through which one can *directly* probe excitation channels—as deviations from elastic scattering behavior. Unfortunately, there have only been a few direct measurements of inelastic losses and yields for the aforementioned Ne^+ systems. In particular, threshold $R_{\min}$ values and yields of Ne^{2+} off the Na→Si target series have not been systematically reported. A review of the limited ISS studies using Ne^+ suggests that excitation mechanisms are still under debate. Binary collision inelasticities (center-of-mass frame) have been reported in a few cases: (1) ~45 eV for Ne^+ (Al and Si) and 75–105 eV ($R_{\min}$ dependent) for Ne^{2+} (Si) when $R_{\min} < 0.47$–0.5 Å [32–34], (2) ~110 eV (no straggling correction) for Ne^{2+} of Si when $E_0 > 2$ keV [35], and (3) ~120 eV (no straggling correction) for Ne^{2+} off Mg/Al/Si with $E_0 = 1.5$–10 keV [34]. The Xu/Baragiola group (case 1, [32,33]) also suggested that Ne^{2+} was due to $2e$-excitation of a non-neutralized projectile in the hard collision where both $4f\sigma$ electrons in the $3d\pi^3 4f\sigma^2$ MO (Ne $2p$) are promoted: $Ne^+(2p^5) + 86\ \text{eV} \rightarrow Ne^{2+*}$. The resulting Ne^{2+*} was thought to transfer an electron to the solid or autoionize to Ne^{2+} far away from the surface. In contrast to the previous view which highly favors double promotion for both the high Ne^+ yield (through Ne^{**} decay) and Ne^{2+} production, Souda *et al.* have continued to maintain that direct reionization ($Ne^+ \rightarrow Ne^0 \rightarrow Ne^+$) is the main contributor to the high Ne^+ yield and argue that doubly excited species are *not* significant in the formation of Ne^+ compared to (re)ionization of Ne^0 [26,36]. In their view, Ne^{2+} is produced via (1) two sequential, one-electron excitations of Ne^0 in consecutive collisions and/or (2) direct ionization of non-neutralized Ne^+ in a single collision. One should note that the aforementioned experiments were conducted at large incident angles (30–60° from the surface plane). On the other hand, work by Guillemot *et al.* (grazing incidence) suggests that a double collision (favorable at grazing incidence), Ne^0 (from AN) → Ne^+ (collision no. 1), followed by production of the Ne^{3+} core in the second collision, is a possible route to Ne^{2+} [17]. Thus it appears that the importance of one-electron excitation events for Ne systems, in the light of both single and double collisions that can generate Ne^{2+}, is still being debated.

Conflicting trends in the scattered ion yield (or intensity) for the $Ne^+ \rightarrow$ Mg/Al/Si systems have also been reported, possibly as a result of the experimental scattering conditions employed, i.e., (1) fixed vs variable angle (θ_{inc}, θ_{exit}, and θ_{lab}) instead of E_0 to probe $R_{\min}$ and (2) reporting the charge fraction, $I/(I+N)$, which includes multiple collision neutrals, versus the scattered ion intensity. Meaningful conclusions about the hard collision step, from the perspective of local neutralization, are hard to make from existing data. Nevertheless, some general observations are worth noting. For experiments where θ_{inc} is fixed (<20°) and θ_{exit} changed, the Ne^+ charge fraction shows both increasing (Mg, Al [17,19]) and up-then-down behavior (Mg [29]) as $R_{\min}$ decreases. Xu *et al.* also observed that the SS-Ne^+ intensity off Si decreases monotonically as θ_{inc} (20–50°, measured up from the surface) increases [32]. This latter trend is puzzling because scattering at grazing angles (small θ_{inc} and θ_{exit}) should favor more neutralization on the incoming/outgoing paths rather than less. The dependence of the Ne^+ intensity (yield) on the actual scattering trajectory suggests that MO promotion and nonlocal neutralization, by themselves, are not likely catch-all explanations. In addition, these two mechanisms, treated separately, ignore the influence of the solid band structure on electronic transitions during promotion [37]. For instance, collision induced neutralization (CIN) can occur where the scattered ion signal (yield) suddenly decreases for $R_{\min}$ less than some critical value [38,39]. In the CIN process, projectile neutralization occurs through resonant tunneling of electrons from the valence band of the target to a partially filled (and promoted) MO. Thus analysis of the scattered ion intensity (yield) behavior as well as inelastic losses with $R_{\min}$ can potentially give strong hints toward which hard collision excitation events are operative and to what extent the collective nature of the surface influences the ultimate outcome of core-level excitation channels. For complex systems involving Ne^+, it is to be expected that projectile velocity, distance from the surface, overlap of energy levels, and the $R_{\min}$ of each binary encounter can all influence the excitation, charge state, and exit kinetic energy of the projectile.

In this paper, we discuss Ne^+ scattering off Mg, Al, Si, and P (GaP) in light of inelastic losses, production of multi-

ply charged scattered ions, and yield trends relating to nonlocal and collision-induced neutralization. Specifically, Ne^+ and Ne^{2+} energy losses and yields are measured throughout the threshold region using fixed scattering geometry by varying the projectile energy (100–1400 eV) to see where core-level excitation channels just begin to turn-on. These experiments were driven by the desire to look solely at the hard collision event while minimizing artifacts (nonlocal charge exchange processes) associated with different trajectory lengths on the incoming and outgoing paths (variable angle studies). We also set out to complete the ISS picture for Ne^+ by carefully looking for the presence of both one and two-electron excitation events as well as use the P target as a test case to evaluate the *Z*-dependence predicted by the MO promotion model for Ne^{2+} production (i.e., the critical $R_{\min}$ decreases going from Mg→P, as dictated by orbital overlap requirements). Three phenomena are seen to occur simultaneously once a critical $R_{\min}$ has been reached in a collision event for Al and Si: (a) opening of the Ne^{2+} channel, (b) reversal in the Ne^+ yield trend which cannot be explained by traditional nonlocal neutralization, and (c) significant hard collision inelastic losses for single-scattered Ne^+ and Ne^{2+}. Some of our threshold and inelasticity measurements agree with the literature while others differ significantly which raises questions about proposed excitation mechanisms. For example, we measure $Q_{bin} \sim 68-75$ eV for Ne^{2+} produced off Si (and Al), notably lower than 85–87 eV reported by Xu *et al.*, which leads us to propose a different mechanism involving $Ne^+ \rightarrow Ne^{+**}$ ($2p^3 3s^2$ or $2p^3 3s 3p$, requiring ~70 eV), that is, a double excitation mediated by the $4f\sigma$ MO. We also observe Ne^{2+} off Al from a single collision event with only 35–40 eV hard collision loss, which matches the direct ionization of Ne^+ to Ne^{2+} (41 eV) and stresses the importance of one-electron ionization/excitation events at the threshold of inelastic channel opening. In addition, similarities for Ne^+ off the P target are drawn to the other systems in terms of the *Z*-dependence of Ne^{2+} production dictated by required orbital overlaps. In the next sections, we present a brief description of the experimental procedure and data analysis, followed by a discussion of the experimental scattering results.

II. EXPERIMENTAL PROCEDURE AND DATA ANALYSIS

A. Experimental procedure

Scattering experiments were conducted in a newly built ion beamline system composed of an inductively coupled plasma source, high-voltage beamline (20 kV) with magnetic mass filter, and deceleration optics to provide isotopically pure ion beam probes for UHV scattering studies [40]. The system produced high fluxes of $^{20}Ne^+$ (>100 $\mu A/cm^2$) at low impact energy [50–1400 eV±5 eV full width at half maximum (FWHM)] onto a grounded target with the scattering chamber in the 10^{-9} Torr range during bombardment. To accurately determine the impact energy, the projectile beam energy distribution was measured directly at the target position using a retractable 180° electrostatic sector and found to be quite Gaussian in shape for energies >50 eV. Scattered species were analyzed using a triple differentially pumped detector system with sequential energy (electrostatic sector) and mass filtering (quadrupole), which enabled the scattered ion energy distributions of all charge states leaving the target to be separately resolved. The exit energy and intensity of Ne^+ and Ne^{2+} were measured in specular reflection for a 45° incident beam, with the electrostatic sector running at constant pass energy (15 eV) and quad with constant Δm (~0.5 amu). Transmission of the sector/quad system was separately calibrated as a function of ion energy using K^+ beams emitted from a hot tungsten wire source floating at different potentials. Finally, a Daly-type ion counting detector on the quad back-end was used to provide ultrahigh counting gain and mass-independent sensitivity. Target samples were Mg, Al (both polycrystalline), Si(100, B-doped), and GaP(111). Each sample was sputter-cleaned at 5 keV (Ar^+), annealed, and amorphized with the Ne^+ ion beam at 300 eV prior to scattering measurements.

B. Analysis procedure

Three aspects of Ne^+ scattering off surfaces are addressed in this paper as a function of collision energy: (a) inelastic losses suffered by Ne^+ in single collision events, (b) opening of the Ne^{2+} exit channel and associated inelastic losses due to local charge exchange phenomena, and (c) changes in the scattered ion yield of Ne^+ and Ne^{2+}. For convenience, the scattering trajectory of the projectile is divided into three steps [1]: (1) approach to the surface, (2) hard collision with a single target atom at small internuclear distance, and (3) recession. On the approach and exit paths, the projectile can experience small inelastic losses due to electronic friction (straggling) with the target valence band—frequently modeled as if the projectile were moving through an electron gaslike layer on the surface. We use the formalism of Oen and Robinsen [41] to calculate the continuous straggling loss (only a few eV in our case) with the fitting parameters (c_i's) of Xu *et al.* [32] and Ascione *et al.* [33]:

$$Q_i = c_i \left(\frac{0.045 A \sqrt{E_i}}{\pi a^2} \right) \exp\left(\frac{-0.3 R_{\min}}{a} \right) \quad [\text{eV}], \tag{4}$$

where Q_i is the straggling loss on paths (1) or (3), E_i is the projectile energy for path (i), $R_{\min}$ is the distance of closest approach, A is a target dependent constant from LSS theory [42], and a is the Firsov or Lindhard screening length [43].

To determine the energy loss associated with excitation during the hard collision step (binary inelasticity $-Q_{bin}$), it is necessary to convert the kinetic energy loss measured in the laboratory to the center-of-mass (c.m.) frame as well as to remove straggling losses. The laboratory-to-c.m. transformation is required because only part of the collision inelasticity is partitioned into the exit kinetic energy loss suffered by the projectile. At 90° scattering angle, the exit energy of the projectile in the laboratory frame (E_{exit}) is given by [1]

$$E_{exit} = K(E_0 - Q_1) - \frac{\gamma}{\gamma + 1} Q_{bin} - Q_3, \tag{5}$$

where E_0 is the projectile incident energy, $K=(\gamma-1)/(\gamma+1)$ is the kinematic factor from elastic scattering theory, and γ is

the target-to-projectile mass ratio (M_t/M_p). Examining Eq. (5), we see that the projectile enters the hard collision with energy E_0-Q_1, scatters elastically off the target atom [where it can suffer a loss of $\gamma/(\gamma+1)Q_{bin}$], and finally leaves the surface after Q_3 is lost on the exit path. Within this framework, inelasticities are evaluated as a function of collision $R_{\min}$ for different targets to determine threshold values where inelastic losses and Ne^{2+} production occur. All $R_{\min}$ values were calculated using the Thomas-Fermi-Molière potential (TFM) [1] with Firsov screening length [43].

Since the ion yield is needed to test model predictions of surface neutralization, the scattered ion intensity signal (detector counts) in the laboratory frame must be converted to a term proportional to the yield. One can write an overall expression for the scattered ion intensity (I_Ω^+) seen by a detector with solid angle Ω as

$$I_\Omega^+ = I_b \rho P^+ (d\sigma/d\Omega)\Omega\eta \tag{6}$$

using the incident beam current (I_b), surface density of scattering centers (ρ), ion survival probability or yield (P^+), cross section ($d\sigma/d\Omega$), and detector efficiency (η) [44]. Rearranging Eq. (6), a term proportional to the yield ($P^+\Omega\eta$) is obtained by normalizing the scattered ion intensity (detector counts) by the incident beam current and differential cross section. All yield data ($P^+\Omega\eta$) presented here have been evaluated in this fashion from the single-scattered ion peak using the TFM potential for the cross section.

III. RESULTS AND DISCUSSION

In the following sections, we summarize Ne^+ scattering off Al and Si in terms of exit energy distributions, laboratory-frame energy losses, and scattered intensities (Ne^+ and Ne^{2+}) as a function of collision energy. Next, we analyze these results with respect to ion neutralization and opening of the Ne^{2+} exit channel on Mg, Al, Si, and P targets. Finally, we calculate collision inelasticities and discuss inelastic loss mechanisms in light of the MO promotion model and surface band structure to make a distinction between one- and two-electron excitation events over different collision $R_{\min}$ ranges.

A. Ne^+ and Ne^{2+} exit energy: Al and Si

Figure 1 shows the measured exit energy of Ne^+ and Ne^{2+} resulting from single binary collisions of Ne^+ with Al and Si targets from ~100–1400 eV, along with the elastic predictions (K=0.149 and 0.167) for single scattering (SS) at 90°. Two regions are seen for both targets where the Ne^+ and Ne^{2+} exit energies are markedly different. At low impact energy (region 1), the SS-Ne^+ exit falls directly on the elastic collision line and no Ne^{2+} is seen in the scattered ion spectrum. Since $R_{\min}$ is relatively large (>0.8 Å at low impact energy for 90° scattering), straggling losses are small (a few eV maximum) and no significant overlap of the core-shell atomic orbitals of the collision partners takes place. As expected, elastic scattering behavior for Ne^+ is seen and no excitation channels exist to form Ne^{2+}. However, as the collision energy is raised (region 2), a transition occurs where

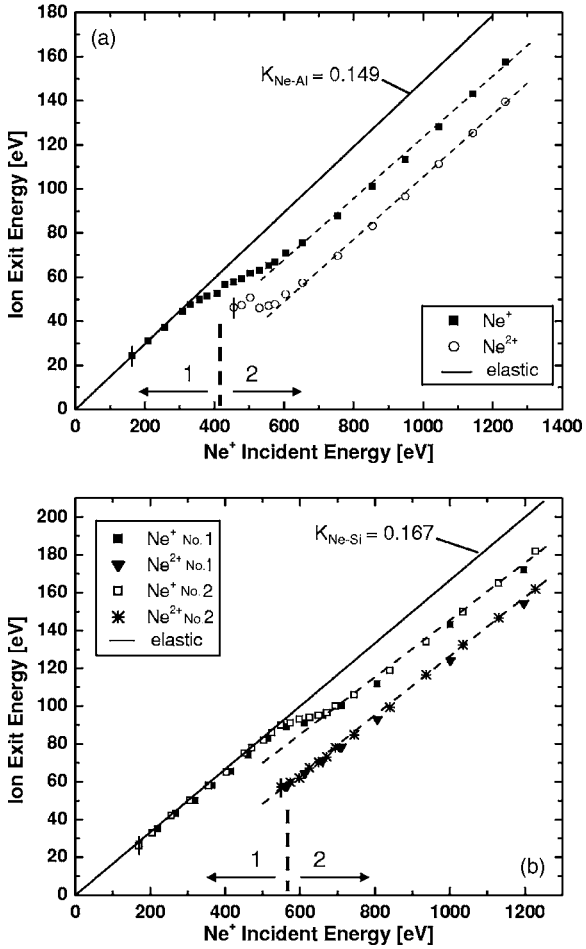

FIG. 1. Exit energies of Ne^+ and Ne^{2+} resulting from single binary collisions of $^{20}Ne^+$ projectiles with: (a) polycrystalline Al and (b) Si (two data sets) for 90° laboratory scattering angle in specular reflection. Elastic scattering behavior for a single collision is indicated with corresponding kinematic factors. Error bars (±5 eV) on the energy data are partially shown to avoid clutter.

the Ne^+ exit becomes inelastic and Ne^{2+} is suddenly generated at ~470 eV impact off Al (550 eV off Si) with a large energy offset from the SS elastic line.

The transition to an inelastic exit is seen more clearly in Fig. 2, where typical raw exit distributions of Ne^+ off Si are shown for several impact energies. The Ne^+ exit peak starts out almost symmetric and well-aligned with the SS elastic position at low-E impact and then transitions to a much broader, asymmetric peak (aligned, but showing some low-E fronting) which is increasingly offset from the SS position as the collision energy is raised. Double scattering events are minimal, as expected for our experiment with large incident and exit angles. Fronting behavior was observed for Ne^+ mainly in the transition region (Al: 300–500 eV and Si: 500–650 eV). To give some measure to this behavior, Ne^+ exit distributions were deconvoluted (Lorentzians) into two peaks which could be identified as SS-like or inelastic depending on the impact energy range (see Fig. 2 inset). At low-E impact, deconvolution results in an SS peak agreeing well with the elastic value, and another lower-energy, inelastic peak that grows in intensity, eventually overtaking the

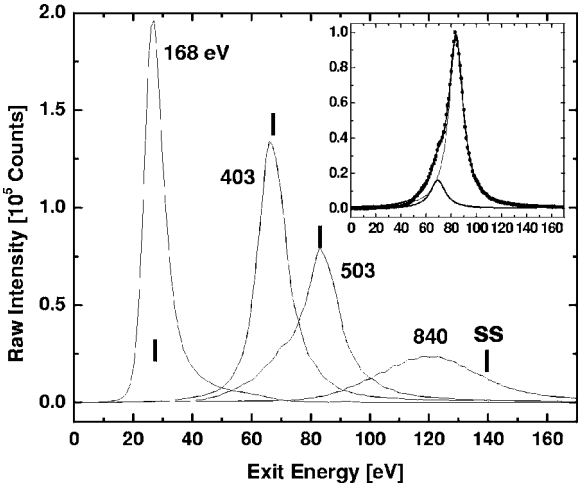

FIG. 2. Scattered ion intensity distributions as a function of exit energy for Ne^+ off Si (100) at 90° laboratory scattering angle at selected incident beam energies (E_0). Raw intensities have been normalized by the beam current and scattering cross section. Single-scattered elastic peak positions are denoted by the SS lines. A representative peak deconvolution for the FWHM analysis is given in the inset for the E_0=503 eV case.

elastic one entirely. Figure 3 shows the results of this deconvolution for an Al target by comparing both the elastic and inelastic Ne^+ FWHMs (extracted from the fit) with those measured for Ne^{2+}. Analogous results were seen for Si. The Ne^+ inelastic exit in region 2 is nearly two times broader than its "elastic" counterpart and Ne^{2+}. Slowly increasing peak widths with impact energy can sometimes be ascribed to system-related effects such as energy or angular spread in the incident ion beam and spread in the scattering angle of the accepted ions due to finite width of detector slits [45]. In our system, the peak width increase is not caused by incident beam spread because its FWHM remained constant at 7–9 eV (180° sector at the target position) over the entire

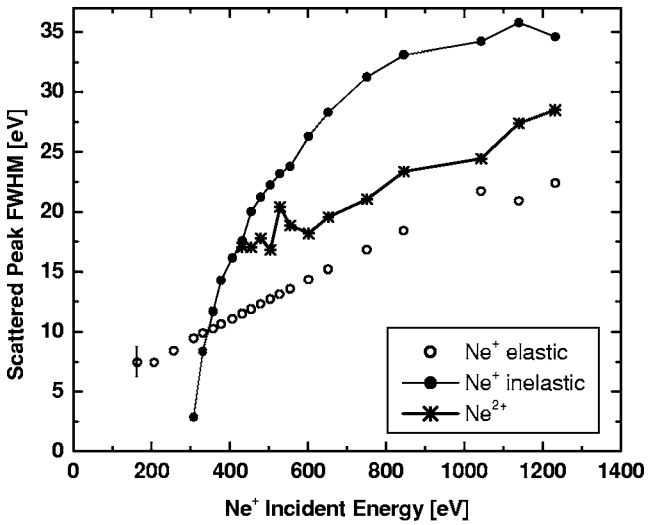

FIG. 3. Measured (Ne^{2+}) and deconvoluted (Ne^+) exit peak widths (full width at half maximum) for scattered energy distributions off Al.

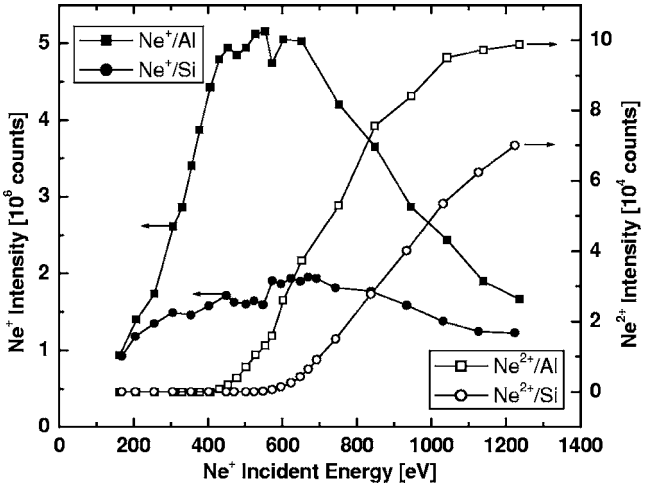

FIG. 4. Scattered ion yields for Ne^+ and Ne^{2+} off Al and Si targets. Only single-scattered events are included.

impact energy range. Angular spread can also be ruled out because (1) the incoming ion beam was skimmed right after the deceleration step (~1 cm from the target) and (2) low-E beams, if anything, should exhibit more angular broadening (and more exit peak broadening) than high-E beams because of space charge repulsion at low energy—however, the inverse trend is seen. Increasing exit width can also be explained on physical grounds: quasisingle (QSS: one glancing, one near 90°) and subsurface scattering [1,46,47] as well as several final states or a continuum into which the projectile/target atoms can be excited. It is difficult to say which process is the most important for Ne^+, but it is rather clear that Ne^{2+} does not descend from multiple collision events (QSS or subsurface) because its width is significantly smaller than that of Ne^+—supporting the view that Ne^{2+} is generated in a single collision event. Analogous jumps in the Ne^+ exit peak width have also been seen by Xu *et al.* for ISS experiments on Si [32]. In addition, since Ne^{2+} production is coincident with Ne^+ inelastic losses and the jump in Ne^+ FWHM, we tend to favor excitation processes over multiple collisions as the cause for the scattering behavior seen in the transition region.

B. Scattered ion intensity and neutralization: Al and Si

The presence of inelastic processes in ion-surface collisions can sometimes be seen indirectly as "dips," oscillations, or a reversal in the ion yield with impact energy (i.e., sudden appearance of CIN or CIR, see Refs. [44,48]). Along this line, we show the scattered yields of Ne^+ and Ne^{2+} off Al and Si in Fig. 4, where the scattered ion intensity has been normalized by the cross section and incident beam current to give a truer picture of projectile ion survival (or conversion). Once again, a distinction between two scattering regions is observed. At first (elastic region), there is a strong increase in the total Ne^+ yield (solid symbols) with impact energy which tends to saturate in the transition region where Ne^{2+} is first generated. Above this threshold, the Ne^+ yield trend reverses and slopes progressively downward, indicating a definite change in neutralization mechanism or opening of an Ne

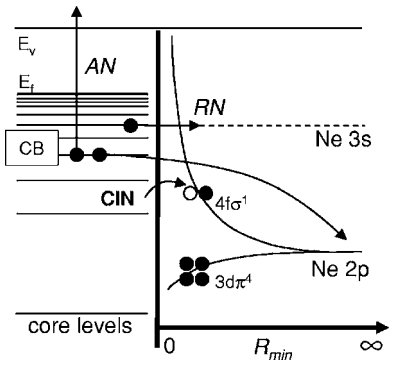

FIG. 5. Schematic representation of projectile neutralization mechanisms for Ne/Ne^+ approaching a surface. RN: resonant neutralization, AN: Auger neutralization, and CIN: collision induced neutralization. Separation of the Ne $2p$ atomic orbital into the bonding $3d\pi$ (demoted) and antibonding $4f\sigma$ (promoted) molecular orbitals is shown as the collision apsis decreases. In this particular case, Ne^+ enters the collision with the vacancy evolving with the promoted $4f\sigma$ MO; however, the collision may also evolve as $3d\pi^3 4f\sigma^2$.

excitation channel(s) that occurs directly in the hard collision itself (i.e., resonant transfer to the $4f\sigma^1$ vacancy, filling the promoted $2p_z$ of Ne^+). During this reversal, Ne^{2+} formation becomes more and more favorable as the impact energy is raised to a point where +2 production represents a non-negligible fraction of the charged Ne species leaving the surface after SS events: roughly $\sim 1/20$ of Ne^+ off Al and $\sim 1/15$ for Si at 1200 eV impact. Plotted in this manner, it is trivial to see the shift in threshold turn-on for Ne^{2+} between Al and Si. Our SS-only yield ratios for Ne^{2+}/Ne^+ are close to those given in Ref. [32] for Ne^{2+} off Si at 1950 eV Ne^+ impact, but significantly smaller than those measured by Souda *et al.* ($\sim 20\%$) [26]. However, it has been noted that the latter authors may not have corrected their intensity measurements for analyzer transmission.

One may be inclined to explain the Ne^+ yield decrease at high-E impact as interconversion of Ne^+ to Ne^{2+}. Although direct conversion is possible, Ne^{2+} formation cannot be the only culprit for the decreasing Ne^+ yield because the Ne^+ intensity change always remains at least an order a magnitude greater than the total Ne^{2+} ever produced. It is perhaps more likely that this decrease is due to CIN via resonant transfer (RT) from the target valence band to the promoted $4f\sigma$ MO (Fig. 5). For instance, if a non-neutralized Ne^+ ($2p^5$) enters the hard collision in the $3d\pi^4$ (demoted) $4f\sigma^1$ (promoted) configuration, RT could easily fill the vacancy as the $4f\sigma^1$ MO crosses into the target valence band. Such an effect is likely unobservable in a glancing angle experiment, where sufficient time exists on the incoming path for the projectile to be neutralized before the hard collision step—effectively removing all possibility of CIN. However, the effective trajectory length available for neutralization of Ne^+ is much smaller in our case at 45° incidence, allowing CIN to be seen by tuning the impact energy through the transition. CIN could only occur if the $4f\sigma$ is strongly promoted, hence a threshold $R_{\min}$ requirement for the decrease in Ne^+ signal. Going one step further, longer time spent by the projectile in the region where the promoted $4f\sigma$ and target valence band overlap should result in an overall higher probability for RT, thus the scattered Ne^+ yield should decrease. These two trends are seen in the scattering data.

Looking back to the elastic region, the increasing Ne^+ signal with collision energy suggests that ion survival is controlled by a decreasing contact time (for electron capture) spent by the projectile in the near-surface region. The high ionization potential for Ne would presuppose that neutralization proceeds by Auger capture rather than resonant transfer [3]. Direct transfer from the conduction band to an excited state ($Ne^* 2p^4 3s$) is possible; however, such a process would be quickly followed by Auger decay involving the surface [3,14]. In either respect, Auger processes are likely to dominate the ion survival probability (P^+) in the elastic region. To test this hypothesis, P^+ can be factored to include contributions from the incoming and outgoing paths (P^+_{in} and P^+_{out}) as well as charge exchange due to CIN (P_{CIN}) or CIR (P_{CIR}) in the hard collision step [49]. A continuum view of Auger neutralization (AN) involving the surface predicts that P^+_{in} and P^+_{out} should scale as $\exp[-v_c/v_{i,\perp}]$ [3,44], where $v_{i,\perp}$ is the projectile velocity perpendicular to the surface and v_c is a characteristic "neutralization" velocity determined by the Auger transition rate (Γ). Furthermore, when CIN and CIR are negligible (i.e., at low-E impact), the survival probability scales as $\exp[-v_c(1/v_{in,\perp}+1/v_{out,\perp})]$. Therefore a semilog plot of the yield (or $P^+\Omega\eta$) versus inverse velocity should give a straight line if nonlocal neutralization controls ion survival. This linear behavior is indeed seen as represented in Fig. 6(a) for Ne^+, where $v_c = 6.4\times10^6$ cm/s for Al and 2.1×10^6 cm/s for Si in the low-E impact limit. We note that such an evaluation for v_c is indeed not a direct determination of the real Auger transition rates involved. In fact, it was mentioned in the Introduction that RN on the exit trajectory involving the Ne $3s$ can be rather important. Extracting an "overall" v_c from the ion yield data is only intended here to highlight differences in neutralization behavior. Nevertheless, similar v_c values have been reported for Ne^+/Mg (4.9×10^6 cm/s) [28] and Ne^+/Si (4×10^6 cm/s) [15] at higher collision energies (2–5 keV) using grazing incidence. When AN is dominant, it is equivalent to change the contact time available for neutralization by varying either incident angle or projectile energy. For the 45° incidence, variable-E case, however, Fig. 6 clearly shows that a transition from nonlocal electron transfer at low-E to some local excitation process (which steals away Ne^+) does occur once a critical $R_{\min}$ is reached. On a final note, one can envision the same type of AN plot for Ne^{2+} [Fig. 6(b)]. The same linear behavior at low-E impact is seen which would suggest that survival of Ne^{2+} (created in the hard collision) is governed by AN or RN on the exit path. We estimate that the "overall" v_c for Ne^{2+} off Si (38×10^6 cm/s) is almost 20 times greater than that of Ne^+.

C. P target

1. Ne^+ and Ne^{2+} exit energy

Since it is not possible to conduct UHV scattering experiments on an elemental P target (high vapor pressure), GaP

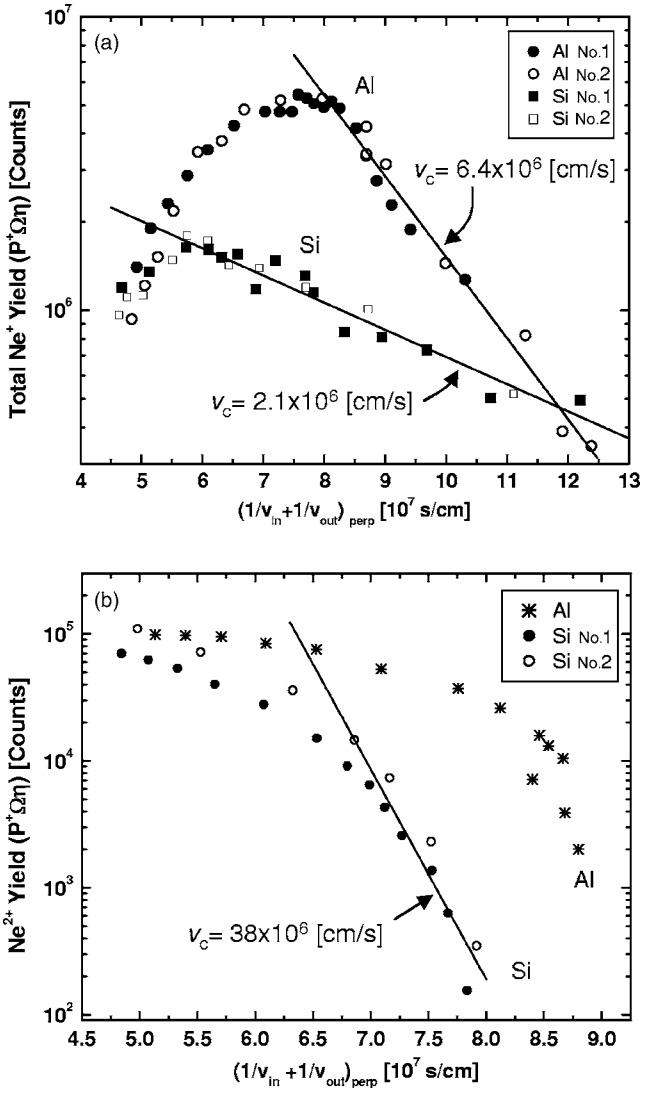

FIG. 6. Experimental determination of the average neutralization velocity (v_c) for low Ne^+ impact energies. The total scattered ion yield ($P^+\Omega\eta$) for (a) Ne^+ (two data sets) and (b) Ne^{2+} off Al and Si is plotted vs the total perpendicular inverse velocity.

(111) was used as a surrogate material to study hard collision excitations in the Ne^+-P system. Figure 7 shows the exit energies measured for Ne^+ and Ne^{2+} off a GaP target for two different runs (random azimuthal orientation), where SS-like scattering behavior from both Ga and P atoms can be seen. The Ne^+ exit off Ga follows the elastic scattering line exceptionally well with minor inelastic losses appearing at high-E impact. On the other hand, the +1 exit off P lies continually above the SS-elastic line, just until the Ne^{2+} exit channel (off P) opens at ~850 eV. Such behavior where one target species is elastic, and the other not, is initially puzzling. This effect cannot be instrument related because the Ne^+ exits off Ga and P are measured simultaneously during the same energy sweep of the scattered product detector. Therefore multiple collision phenomena must be involved for the P atom case. Indeed, exit energies higher than BCA can only be explained through multiple deflections of the projectile, i.e., for a double collision, $K_{Ga}(\theta)K_P(90°-\theta)$ with $\theta<90°$ is always larger (higher exit energy) than the kinematic factor for a single 90° defection off P alone. The question then becomes why does such behavior occur. Looking at the sputtering literature on III-V materials reveals that ion bombardment can induce a significant change in the stoichiometry of surface layers due to differences in sputtering yields. For example, changes on the order of $Ga_1P_{0.6-0.7}$ have been measured by XPS and He^+ ISS after mild ion bombardment of GaP monocrystals [50]. This situation suggests that an Ne^+ projectile would have to interact with or traverse a Ga-rich surface to scatter off a P atom in the present case. Incidentally, the linear Ne^+ behavior off P below 800 eV can easily be fit with a glancing double event, where the first deflection off Ga is ~4° (K=0.999, effectively no loss), followed by 86° off P (K=0.243), giving rise to a larger kinematic factor (0.242) than for single-scatter at 90° (0.216). Clearly, this explanation is a greatly simplified view of the deflection dynamics; however, it is useful to ask why a glancing interaction with Ga might occur in most cases before a large angle deflection off P. Although the GaP surface is amorphized to some extent during bombardment, low projectile energies should not significantly disturb the overall crystalline nature of the layers just below the immediate target surface. Figure 8 gives a schematic representation of an incoming trajectory path that could sample a second layer P atom (θ_{lab}=90°) for an ion at 45° incidence on a Ga-terminated GaP(111) surface. In this scattering configuration, if a P atom is sampled, irrespective of the azimuthal entrance angle (in the 111 plane), the projectile would likely experience a small deflection before the large angle P collision due to stronger interaction with Ga atoms on the leeward side of the approach path (to the right of the incident beam direction). Although the very top surface layer is surely not crystalline, the scattering data would suggest that some underlying organization to the GaP

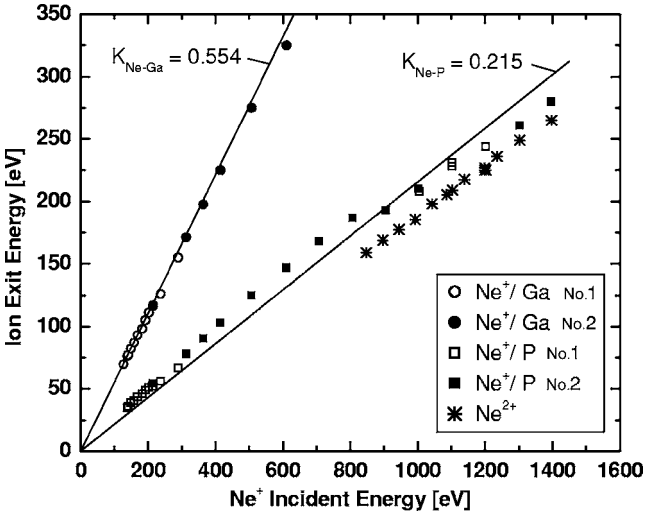

FIG. 7. Exit energies of Ne^+ and Ne^{2+} off a GaP (111) target showing the $\langle E_{exit}\rangle$ for deflection events off Ga or P atoms. The corresponding kinematic factors for a single, elastic 90° deflection off Ga or P are indicated. Labels no. 1 and no. 2 represent two different scattering experiments for an unknown, random azimuthal alignment (angle in the 111 plane) for the incoming Ne^+ beam. Error bars for the exit energy are roughly the symbol size.

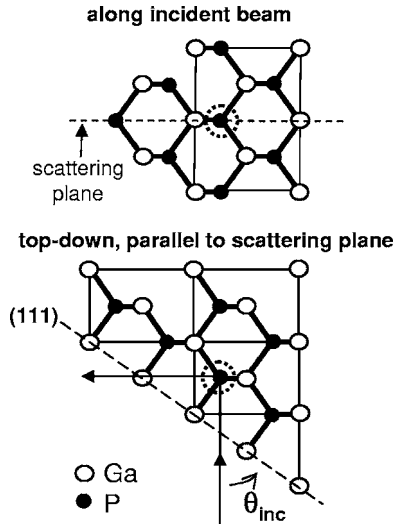

FIG. 8. 2D projections of the experimental scattering geometry for projectiles impacting a Ga-terminated GaP (111) surface at $\theta_{inc}=45°$ and $\theta_{lab}=90°$. The incident ion trajectory which can sample second layer P atoms (dotted circle) through a 90° deflection is shown. The azimuthal angle is measured in the 111 plane (dashed line, bottom panel).

"lattice" still exists to the extent that there is a preferred multiple collision sequence involving P. Further scattering experiments with the primary beam aligned along particular azimuths and shadow cone studies by changing θ_{inc} are underway to try to better understand this behavior. Indeed, it is a little surprising that a "semi-amorphous" surface, possibly enriched with Ga atoms, can give P atom ISS peaks consistently above the elastic line.

Although the underlying cause of Ne^{2+} is more difficult to extract in a binary target case, we have already seen that Ne^{2+} production off GaP is strikingly similar to the other Ne-light target cases studied—suggestive that the +2 exit is driven by *L*-shell interaction of Ne with P, rather than Ga. Further evidence for this claim comes from an examination of the one-electron MO correlation diagrams for Ne+P and Ne+Ga (Fig. 9), constructed using the Barat-Lichten rules [21] for correlating the separate atom and united atom electron states. For Ne+P, we can see that the highly promoted $4f\sigma$ associated with the Ne $2p$ crosses MOs of like symmetry arising from the P $3s$, Ne $3s$, and P $4s$. Such crossings with the Ne $3s$ are potential routes to Ne^{+**} $(2p^3 3s^2)$ and Ne^{2+*} $(2p^3 3s)$, which can autoionize and eventually be detected in the scattered ion spectrum as Ne^{2+}. However, in the Ne+Ga case, the $4f\sigma$ from the Ne $2p$ crosses the Ga $4s \rightarrow$ Nb $4s$ MO at larger internuclear distance than that of the Ne $3s \rightarrow$ Nb $4p$. This latter observation would suggest that excitation to the Ga $4s$ should be more favorable than for the Ne $3s$, supporting the position that excitation involving the Ne $3s$, which is only accessible in the Ne+P case, is the root cause of Ne^{2+} off the GaP target at low collision energies. Another difference in the Ne+P and Ne+Ga cases is promotion of the Ne $2s$ (Ne $2s \rightarrow$ Mn $3p$ vs Ne $2s \rightarrow$ Nb $3d$). Crossings involving the Ne $2s$, i.e., to the P $3s$ or Ga $4s$ may be important, but smaller internuclear separations (higher collision energy) would be required; additionally,

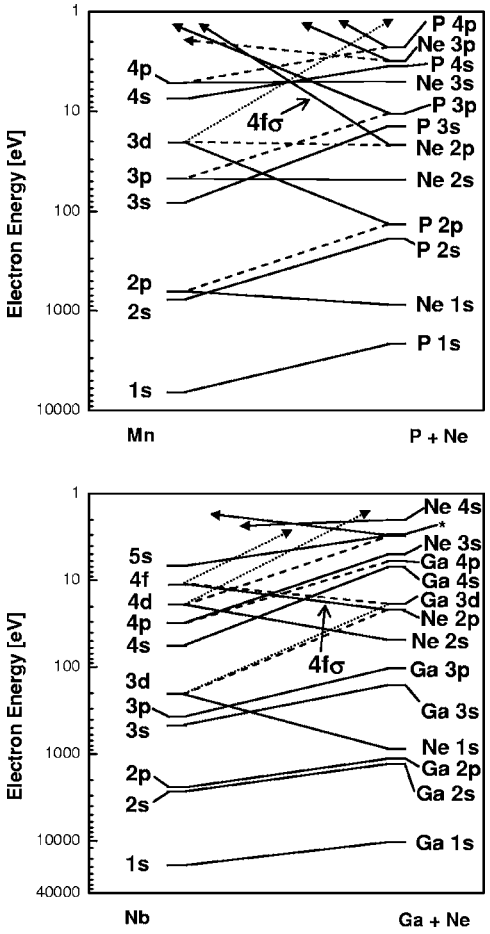

FIG. 9. One electron MO correlation diagrams for Ne+P and Ne+Ga. In these diagrams, the outer electron levels for the metals are only indicative of where they might be expected to be found within the electronic continuum. Solid, dashed, and dotted lines represent the σ, π, and δ molecular orbitals, respectively. The * label refers to the overlapping Ne $3p$ and Ga $5s$ states.

these crossings would not give access to the formation of excited Ne $3s$ states. All in all, it would seem that Ne^{2+} off GaP descends from the Ne+P interaction, rather than Ne +Ga.

2. Scattered intensities

Typical exit energy spectra for Ne^+ off GaP are given in Fig. 10. Reversal in the scattered peak intensities can be seen as the impact energy is raised. This trend, although not specifically discussed, is also seen in the ISS spectra of Tolstogouzov *et al.* for Ne^+ off GaP [51]. In fact, the Ne^+ exit off P becomes more dominant than its Ga counterpart at energies above 300 eV for our 90° laboratory scattering angle. Intuitively, the exit off Ga should be more favorable at low-*E* impact because of the aforementioned Ga-rich surface and minimal penetration of the projectile into the lattice. Figure 11 shows a summary of how the exit intensities of Ne^+ peaks off Ga and P change with energy, along with the Ne^{2+} signal. For this data, the exit intensity has been normalized by the beam current, but not corrected for the cross-section dependence because of the unknown collision history for the Ne^+

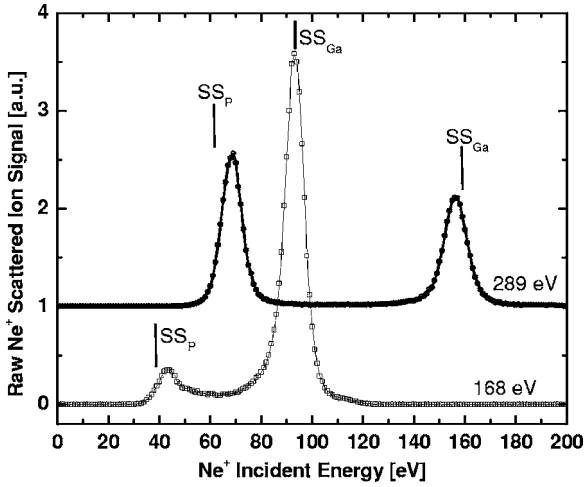

FIG. 10. Exit energy distributions of Ne^+ off GaP showing the single-scatter exits off Ga and P.

exit off P (i.e., multiple collisions). The incident beam current was also kept as constant as possible (3.5–5.5 μA) over the entire energy range to try to remove any fluence-related artifacts. A more intense +1 exit off P compared to Ga is opposite to the expected cross-section dependence ($\partial\sigma \sim Z^2_{\text{target}}$). However, the increased P signal relative to Ga may be due to ion focusing effects. In fact, a quick look back at Fig. 8 shows that a triangular lattice of Ga atoms lies just above (in front of) every P atom site for our incidence geometry. These three atoms could provide a natural funneling affect for incoming ions. Similar effects due to ion focusing have been seen for Ne^+ scattering off GaAs (110) [52].

D. Ne^{2+} production: All targets

The sharp onset of Ne^{2+} production with increasing collision energy for all the targets tested is clearly indicative of an excitation mechanism that opens below some critical R_{min}. Naturally, one would surmise that this turn-on point should depend directly on the Z of the target atom if electron transfer to and from promoted MOs during the hard collision step is responsible. To this end, the turn-on of Ne^{2+} was measured for Mg, Al, Si, and P (GaP) targets, and found to be ~450, 500, 700, and 850 eV, respectively. These threshold energies correspond to R_{min} values of ~0.65, 0.64, 0.57, and 0.51 Å at 90° laboratory angle using the TFM potential. The decreasing R_{min} requirement for a heavier target is illustrated in Fig. 12, where normalized Ne^{2+} signals are shown. If a similar MO curve crossing was involved in Ne^{2+} production for all the targets, a decreasing R_{min} requirement for the Ne^{2+} turn-on should be seen since the AOs of the target atom pull closer to the nucleus with increasing Z. In fact, curve crossings on an MO correlation diagram are analogous for Ne–Mg through Ne–P because the electron binding energies of Mg through P do not change energy ordering with those of Ne. Hence strong promotion of the $4f\sigma$ MO at similar crossing points, if this is the trigger for Ne^{2+}, should occur at smaller separation as Z increases. This trend is clearly observed in the data.

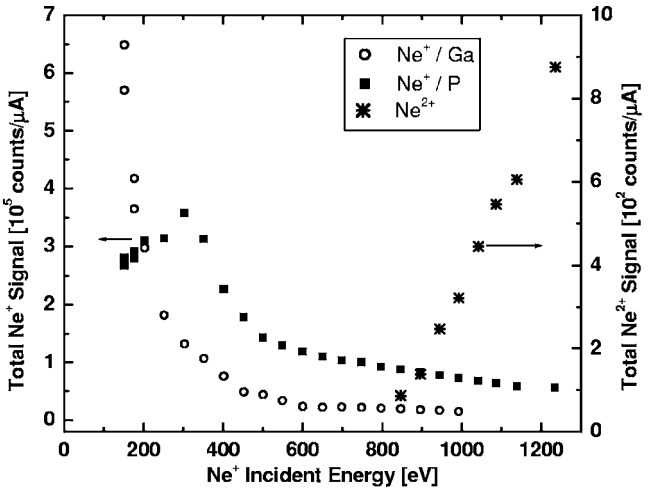

FIG. 11. Raw intensity signal (normalized by the beam current) for the SS exits of Ne^+ and Ne^{2+} off Ga and P atoms in the GaP target.

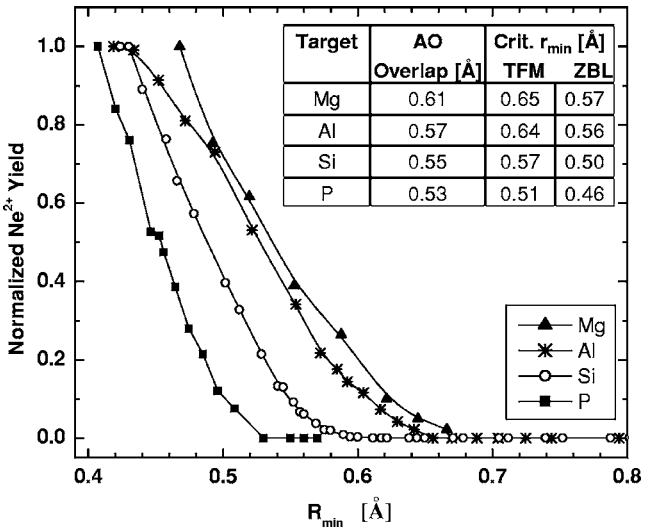

FIG. 12. Normalized Ne^{2+} yield off Mg, Al, Si, and P targets for $^{20}Ne^+$ projectiles. The data shown represent the Ne^{2+} yield, normalized by the maximum for each target. The inset gives the theoretical orbital overlap distance of the L-shell of the target with the Ne $2p$ and the Ne^{2+} turn-on R_{min} point using the TFM and ZBL potentials.

To go a step further, we can evaluate the AO overlap from a more theoretical point of view. The mean distance for maximum density in the radial wave function is useful in this respect [53]. Overlap of the Ne $2p$ AO with the target L-shell (mean $2s-2p$) should occur for separations near ~0.61, 0.57, 0.55, and 0.53 Å for the Ne–Mg, Ne–Al, Ne–Si, and Ne–P pairs. The inset in Fig. 12 shows a comparison of the theoretical overlap with the Ne^{2+} turn-on R_{min} from the experimental data using the TFM and ZBL (Ziegler-Biersack-Littmark) potentials. Agreement between the theoretical overlap and experimental R_{min} required for Ne^{2+} production is good—within the sensitivity of the potential and screening length used to determine R_{min}. It seems clear that overlap of the Ne $2p$ AO with the L-shell of the target atom is a sufficient condition for strong MO promotion (through the $4f\sigma$ from the Ne $2p$), such that Ne^{2+} formation occurs for the four

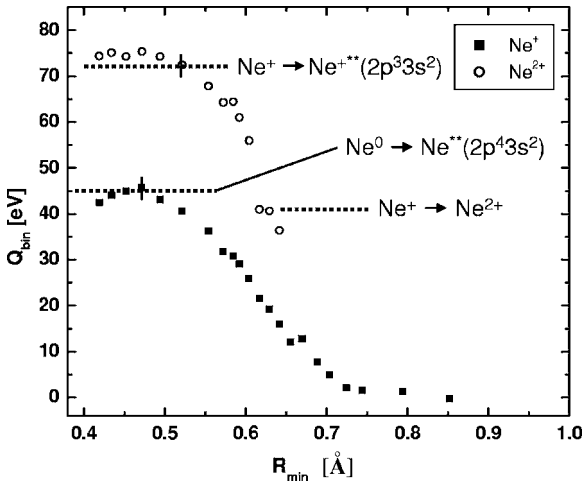

FIG. 13. Hard collision inelasticities for Ne^+ and Ne^{2+} resulting from Ne^+ impact on Al. $R_{\min}$ is determined with the TFM potential. Transition energies for several Ne^0 and Ne^+ excitation mechanisms mentioned in the text are also shown.

targets. Coincidentally, this overlap requirement seems to also trigger Ne^+ inelasticity as well as the Ne^+ yield downturn.

On a final note, we should comment on the potential effects of surface roughness on the scattered Ne^{2+} intensity for the different targets. It has been shown recently via electron spectroscopy that the Ne^{**} Auger yield (autoionization decay) is significantly affected by surface topography for grazing incidence scattering [20]. It was seen that smooth surfaces tend to "spoil" (lower intensity and more broad) autoionization decay lines because an excited projectile spends more time near the surface than for a rough case, i.e., autoionizing states can be depopulated more easily due to closer interaction with the smooth surface. Although we did not specifically evaluate surface roughness in our case, we believe that our target surfaces were rough due to Ar^+ bombardment at 5 keV during the initial surface cleaning procedure. Whatever the roughness of a given target surface, the Ne^{2+} yield data were reproducible after cleaning and the scattered species intensities did not change even after appreciable scattering time (hours) on that surface. In any event, if Ne^{2+} descends from an autoionizing precursor (which appears to be the case—see the next section), the large incident angle and on-average, rather rough surfaces used in the present case would seem to cancel out any target-to-target differences in yield due to surface topography.

E. Inelasticities

Significant deviations from elastic behavior were seen in Fig. 1 (region 2) for Ne^+ and Ne^{2+} off Al and Si targets. These laboratory-frame losses can be converted to hard collision inelasticities using the analysis method mentioned in Sec. II B to compare with discrete electronic excitation channels for the projectile and/or target atoms. Results of this conversion are summarized in Fig. 13 for Ne^+ and Ne^{2+} off Al (Si results are nearly identical). In general, Q_{bin} values for both exits steadily increase as $R_{\min}$ decreases until saturation behavior occurs for $R_{\min}$ below $\sim 0.5-0.55$ Å. Our values for Ne^+/Al and Si in the saturation region are right on par with the 45 eV loss needed to form Ne^{**} in the hard collision from an Ne^+ that has been neutralized to Ne^0 on the incoming path. The wealth of electron spectroscopy data relating to Ne^{**} decay, along with the correspondence between energy losses measured in the present work and other ISS studies in literature, verify that the $Ne^0 \rightarrow Ne^{**}$ double promotion transition is beyond debate. Evidence for direct ionization of Ne^0 to Ne^+ ($Q_{bin} \sim 22$ eV), as some propose [26], has yet to be found in both our work and that of Xu *et al.* [32].

Concerning Ne^{2+} production, several mechanisms have been suggested in the literature: (1) double promotion of a non-neutralized Ne^+ ($Ne^+ + 86\ eV \rightarrow Ne^{2+*} + e^-$), (2) two, one-electron excitations of Ne^0 in consecutive collisions, and (3) direct ionization of Ne^+. With respect to Ne^{2+} inelasticities, our measurements show Q_{bin} values for Al (and Si) in the 68–75 eV range—considerably lower than the 84.9 or 87.5 eV requirement for double excitation of Ne^+ to Ne^{2+*} [$2p^3(^2D, ^2P)3s$, lying 106–109 eV above Ne^0] previously reported [32]. Since our Ne^+ values agree quite well with other ISS studies, it is difficult to explain why this difference in Q_{bin} for Ne^{2+} occurs. We note here that the study of Xu *et al.* [32] for Ne^{2+} off Si, where +2 production was discussed in detail, was conducted using variable angles (θ_{inc}, θ_{exit}, and θ_{lab}) at several fixed projectile energies (500, 700, 100, 1400, and 1950 eV) to sample different $R_{\min}$. Careful examination of their data shows, for fixed projectile energy, that Q_{bin} for Ne^{2+} changes by some 20 eV, depending on what laboratory scattering angle is used (θ_{inc} and θ_{exit} are changing also). This trend could indicate that straggling losses are not only $R_{\min}$ dependent [through Eq. (4)], but they also vary with the specific trajectory path on approach or exit from the hard collision. As such, determining Q_{bin} using scattering angle to sample $R_{\min}$ is complicated by how to correctly remove the straggling loss component when θ_{inc} and θ_{exit} are changing. The angular dependence and large variance in Q_{bin} values for the former work attest to this fact. On the other hand, these problems are absent from our experiment because $R_{\min}$ is sampled by only changing the incident energy at fixed angle; thus the incoming and outgoing trajectory paths are always the same.

Having said this, we suggest the Ne^+ to Ne^{+**} ($2p^3 3s^2$ or $2p^3 3s 3p$, 90.3–93.3 eV above Ne^0) transition involving $4f\sigma$ double promotion as the route to inelastic Ne^{2+} in the Q_{bin} saturation region. Since Ne^+ is 21.6 eV above Ne^0, the $Ne^+ \rightarrow Ne^{+**}$ transition would give Q_{bin} values of 68.8–71.7 eV, which agree very well with our data. Even more evidence for this assignment can be found in Auger spectra taken during Ne^+ scattering off Al(111). Careful analysis of Auger peaks occurring at energies higher than the two main Ne^{**} lines lead Xu *et al.* to conclude that decaying $2s^2 2p^3 nln'l'$ states (Ne^{+**}) were involved [14]. Formation of the $2s^2 2p^3$ core can occur if the projectile has a vacancy in the $2p$ and that vacancy evolves with the demoted $3d\pi$ MO (i.e., hard collision occurs with $3d\pi^3 4f\sigma^2$). Both these conditions can be met for an Ne^+ which survives neutralization on the incoming path. Since Ne^{+**} descends from a non-neutralized projectile, scattered Ne^{2+} should be significantly less intense than Ne^+ because of the high neutralization rate for Ne^+ on

the incoming path. This large intensity difference is exactly what is seen (refer to Fig. 4). Furthermore, energy loss values for Ne^{2+} and nearly identical K values (slopes) between Ne^{2+} and SS-Ne^{+} (E_{exit} vs E_0, the elastic BCA line in Fig. 1) give no reason to think that Ne^{2+} results from a double collision sequence involving Ne^0 as proposed by Souda *et al.* [26]. In our opinion, double collision sequences should not show such "nice" correspondence with the SS-elastic trend in terms of both the E_{exit} vs E_0 data and narrow scattered peak widths (Fig. 3). For direct ionization of $Ne^0 \rightarrow Ne^{2+}$ ($\sim$62 eV), it would also seem from the Q_{bin} data that this route can be eliminated for the saturation region.

Next, we move to the interesting feature for Ne^{2+} off Al at $Q_{bin} \sim 40$ eV. In fact, the presence of SS-Ne^{2+} with $Q_{bin} < 70$ eV casts doubt on the view that two-electron excitation of Ne^+ is the only route to Ne^{2+} as previously discussed [32]. We must therefore consider one-electron events. Starting with Ne^+ or Ne^*/Ne^{+*} (formed on the incoming path), several one-electron events can lead to Ne^{2+}—directly in the hard collision or as a result of charge exchange on the exit path. For example, one can envision: (a) direct ionization of surviving Ne^+ ($2p^5$) to Ne^{2+} ($2p^4$) ($\sim$41 eV), (b) $Ne^* \rightarrow Ne^{2+}$ with 46 eV loss, (c) $Ne^+ \rightarrow Ne^{+*}$ ($2p^4 3s$) taking $\sim$27.3 eV, followed by resonant ionization to the target bands on the exit path, or (d) single excitation of Ne^{+*} ($2p^4 3s$) to Ne^{+**} ($2p^3 3s 3l$) requiring $\sim$41–45 eV, then autoionization to give Ne^{2+}. As the simplest mechanism, direct ionization should be considered first. Let us suppose that the hard collision occurs with an Ne^+ that has survived neutralization on the incoming path and the collision partners approach with the Ne $2p$ AO evolving into the $3d\pi^3 4f\sigma^2$ MO configuration. When the $4f\sigma$ MO is highly promoted, an electron can be resonant ionized to empty band states of the target, creating a $3d\pi^3 4f\sigma^1$ situation (Ne^{2+}). The demoted vacancy in the $3d\pi$ is irrelevant in this case because it cannot be filled. Such a mechanism would result in Ne^{2+} with Q_{bin} $\sim$41 eV (ionization potential of Ne^+) if the electron were released at the vacuum level or as little as $\sim$36 eV (41–4.9 eV work function for Al) if released at the first empty conduction band states. Interestingly, Ne^{2+} off Al is seen in Fig. 13 with Q_{bin}=35–40 eV at the +2 turn-on point. As well, Souda *et al.* have pointed out that electrons released to the conduction band are hardly returnable to the projectile because of the rapid diffusion of the electron into the band itself (i.e., diffusion time $\sim 10^{-16}$ s vs collision time $> 10^{-15}$ s [54]). Occupancy of the $4f\sigma$ is therefore determined on the PE curve descent by resonant tunneling from the target valence band. In fact, there seems to be no other way to create Ne^{2+} in an SS event off Al with only 40 eV hard collision energy loss. We must conclude then that in the threshold region, Ne^{2+} most likely results from single-electron excitation of surviving Ne^+, transitioning to a two-electron process for small R_{min}. Gas-phase collisions involving Ne support this hypothesis. Barat and co-workers have shown for gas-phase Na^+–Ne collisions that both one-electron and two-electron ionization/excitation of Ne occurs depending on the collision R_{min} [55]. Once the turn-on threshold is reached, one-electron events take place over a narrow range, and then transition into two-electron events as R_{min} decreases further. Thus it appears that one-electron transitions may be more important in our case for the threshold region where Ne^{2+} just begins to form at large R_{min}.

At this point, the only region left to explain is the 55–60 eV loss for Ne^{2+} seen at intermediate R_{min}. We are unsure how to attribute a well-defined excitation channel to this region because a careful look at transitions from Ne^*, Ne^+, and Ne^{+*} to higher states which could yield Ne^{2+} gives Q_{bin} values either significant lower or higher than $\sim$60 eV, except for perhaps $Ne^{+*}(2p^4 3s)$ to $Ne^{2+*}(2p^3 3s)$ requiring 58–61 eV. Although we feel that this transition is rather unlikely, we cannot rule it out. We should also mention the possibility of a double collision event for the $\sim$60 eV loss. Indeed, a double collision where $Ne^0 \rightarrow Ne^+$ (direct ionization, $\sim$20 eV), followed by $Ne^+ \rightarrow Ne^{2+}$ (direct ionization, $\sim$40 eV), would seem a rather convenient explanation for the 60 eV loss case. However, direct ionization in the hard collision (promotion to vacuum) would presuppose that R_{min} is rather small, i.e., a nongrazing first collision, followed by a nongrazing second collision to give a 90° exit. For both these nongrazing collisions, and in fact, any double collision, the overall kinematic factor ($K_\alpha K_{90-\alpha}$) is always greater than K_{90° for a single collision. As such, a double collision exit seen at 90° laboratory angle should be considerably higher in exit energy (even with Q_{bin} loss) than the single-scatter case—which is not reflected in the energy loss data. Thus the double collision route appears improbable.

Perhaps an explanation of the Ne^{2+} loss in this intermediate region is intimately related to a larger discussion of why an increasing inelasticity trend occurs. Indeed, direct ionization of Ne^+ to Ne^{2+}, which would seem probable for Ne^{2+} off Al at the +2 turn-on, may be the underlying cause of Ne^{2+} for the 60 eV loss case—if one could explain why Q_{bin} increases as the R_{min} gets smaller. Although the latter trend has been seen before [32], an explanation for it is still lacking. We highlight here some effects, which may contribute to the increasing Q_{bin} behavior. Energy level shifting and broadening of metastable and ionic states of the projectile are known to occur during the projectile approach to the surface [3,25]. Electron transitions involving these states could be responsible for steadily increasing inelastic losses because energy level up-shifting and broadening both become more pronounced as R_{min} decreases. Interestingly, the smoothly increasing inelasticity trend seems almost too reminiscent of the rise in the $4f\sigma$ PE curve (see Fig. 5). In this sense, the promoted $4f\sigma$ may act as an electron "shuttle" by sinking electrons from the valence band through resonant transfer on the PE curve ascent, subsequently dumping these electrons into empty conduction band states or carrying them all the way to the vacuum level. Thus the increasing inelasticity would be due to target excitations where the valence band electron, which fills the incoming ion vacancy, is deposited at increasingly higher potential energy dictated by the turning point on the $4f\sigma$ PE curve—which indeed becomes continuously higher in energy as R_{min} decreases.

Finally, we should comment on inelastic losses for the GaP target. Attributing a particular hard collision excitation mechanism to inelastic losses is much more difficult for the Ne^+–P case because multiple collision processes may be involved. In addition, it is not immediately apparent how to

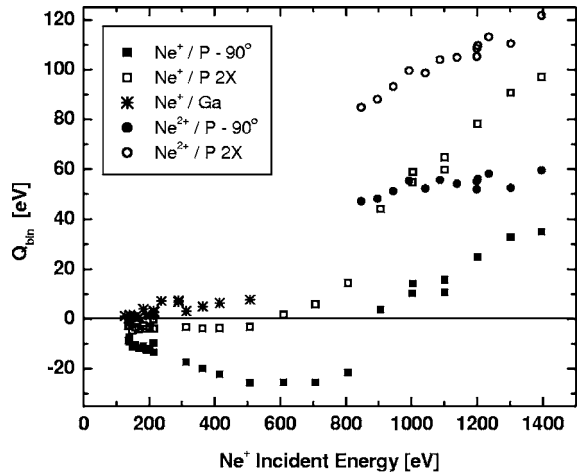

FIG. 14. Hard collision inelasticities (without straggling correction) for Ne^+ and Ne^{2+} off GaP. The 90° data are calculated for a single 90° deflection off Ga or P and the points denoted ($2\times$) are evaluated assuming a double collision event where the projectile is scattered first at 4° off Ga and then 86° off P. See text for details. Error bars for Q_{bin} are slightly larger than the symbol size.

evaluate straggling losses for a binary target when the projectile may have to traverse a Ga-rich surface before encountering P atoms where the subsequent large angle deflection occurs. It is useful nonetheless to consider the overall magnitude of inelastic losses to compare with the other targets studied. In this respect, we have evaluated Q_{bin} for two separate scattering configurations (Fig. 14): (1) a single 90° deflection off Ga or P and (2) a glancing, double collision event with Ga at 4°, followed by 86° off P as discussed in Sec. III C 1. Ne^{2+} was assumed to result from the P collision only and no straggling losses have been removed from the raw Q_{bin} data. If multiple collisions are involved for the Ne^+ and Ne^{2+} exits off P, Q_{bin} values referenced to a 90° deflection can only be thought of as a lower bound to the hard collision loss. Likewise, the 4°-then-86° double collision event poses an upper bound, assuming that the same trajectory combination occurs over the energy range studied. Given these constraints, it is seen that the hard collision excitation process which generates Ne^{2+} (or the excited state precursor which is finally detected as Ne^{2+}) involves energy losses in the 50–100 eV range. This range would indeed capture all double promotion processes of an Ne^+ to final states with a $2p^3$ core—certainly not excluding the same $4f\sigma$ MO promotion process discussed earlier. In any event, it is apparent that the Ne^+-P case has striking similarities with other light target systems from the perspective of a well-defined Ne^{2+} turn-on, continually increasing Ne^{2+} yield with impact energy, and rather constant Ne^{2+} energy offset from the SS-elastic line. Clearly, Auger spectroscopy during Ne^+ bombardment of GaP could help answer these outstanding issues.

IV. CONCLUSIONS

In summary, we have studied charge exchange phenomena for energetic Ne^+ collisions with Mg, Al, Si, and P targets across the threshold impact energy region where inelastic losses in hard collision events are first observed. Experiments were conducted in a fixed scattering geometry by changing only the impact energy to probe different $R_{\min}$ in an effort to minimize the influence of the trajectory path on nonlocal charge exchange before and after the hard collision event. At low energy, Ne^+ scattering is seen to be purely elastic and the ion yield is well explained by a continuum Auger-type neutralization model. In this sense, ion survival is dictated by nonlocal electron transfer from the Fermi sea of the target to the projectile during the approach to and exit from the surface. However, when the Ne^+ impact energy is raised above a specific threshold (critical $R_{\min}$), three phenomena occur simultaneously in the scattered ion spectrum for single collision events off Al and Si: (1) Ne^{2+} generation, (2) reversal of the Ne^+ yield trend with impact energy, and (3) significant hard collision losses in both Ne^+ and Ne^{2+} exit channels. Although the collision dynamics off GaP showed that multiple deflections may be important, analogous behavior for the Ne^+–P system was seen from the perspective of sizable hard collision losses for Ne^{2+} and a well-defined +2 turn-on. In all cases, $R_{\min}$ values for the onset of Ne^{2+} production agree well with the theoretical distance required for overlap of the L-shells of the projectile and target atoms, demonstrating the expected Z-dependence of excitation. As such, transitions involving the $4f\sigma$ MO are likely responsible for all three events where the exit charge state of the projectile is determined by both core-level interaction and resonant/Auger transfers on the exit trajectory. Regarding the Ne^+ ion yield, a clear transition from nonlocal neutralization at low-E impact to $R_{\min}$-dependent collision induced neutralization behavior was seen for SS events in the Al and Si cases. Finally, hard collision inelasticities were measured for Ne^+ and Ne^{2+} off Al and Si in the threshold region. In the high impact energy limit, inelasticity values approach those reported in the literature for two-electron excitation of Ne^0 to Ne^{**} (45 eV); however, saturation values for Ne^{2+} were found to be lower (68–75 eV) than those published for Ne^{2+} off Si (85–87 eV). We attribute Ne^{2+} production at high-E impact to the $Ne^+ \rightarrow Ne^{+**}$ ($2p^3 3s^2, 2p^3 3s3p$) double promotion transition involving the $4f\sigma$ MO, which fits our Ne^{2+} energy loss data very well. Remarkably, at large $R_{\min}$, energy losses for Ne^{2+} off Al were seen to start at 35–40 eV. Such values for Q_{bin} cannot be explained from the perspective of two-electron excitation events. Direct ionization of a surviving Ne^+ in a single-electron event to form Ne^{2+} (Q_{bin} = 36–41 eV) is proposed as a more likely mechanism for intermediate $R_{\min}$ values in the Al target case.

ACKNOWLEDGMENTS

We express our gratitude to Mike Roy in the Caltech chemistry machine shop for his design assistance and tireless hours of fabrication. This research work was funded in part by the NSF (CTS-0317397) and Applied Materials. Additionally, M. Gordon would like to thank the Intel Foundation and Applied Materials for personal scholarship support.

[1] J. W. Rabalais, in *Principles and Applications of Ion Scattering Spectrometry: Surface Chemical and Structural Analysis* (Wiley, New Jersey, 2003).

[2] S. R. Kasi, H. Kang, C. S. Sass, and J. W. Rabalais, Surf. Sci. Rep. **10**, 1 (1989).

[3] H. D. Hagstrum, in *Inelastic Ion-Surface Collisions*, edited by N. H. Tolk, J. C. Tully, W. Heiland, and C. W. White (Academic Press, New York, 1977), p. 1. See also H. Hagstrum, Phys. Rev. **96**, 336 (1954).

[4] R. A. Baragiola, Radiat. Eff. **61**, 47 (1982).

[5] E. W. Thomas, Vacuum **34**, 1031 (1984).

[6] T. M. Buck, G. H. Wheatley, and L. K. Verheij, Surf. Sci. **90**, 635 (1979).

[7] J. W. Rabalais, J. A. Schultz, R. Kumar, and P. T. Murry, J. Chem. Phys. **78**, 5250 (1983).

[8] A. J. Algra, E. van Loenen, E. P. Th. M. Suurmeijer, and A. L. Boers, Radiat. Eff. **60**, 193 (1982).

[9] W. Eckstein, V. A. Molchanov, and H. Verbeek, Nucl. Instrum. Methods **149**, 599 (1978).

[10] S. B. Luitjens, A. J. Algra, E. P. Th. M. Suurmeijer, and A. L. Boers, Surf. Sci. **99**, 631 (1980).

[11] W. Heiland and E. Taglauer, Nucl. Instrum. Methods **132**, 535 (1976).

[12] R. Kumar, M. H. Hintz, and J. W. Rabalais, Surf. Sci. **147**, 15 (1984).

[13] G. Zampieri, F. Meier, and R. Baragiola, Phys. Rev. A **29**, 116 (1984).

[14] F. Xu, N. Mandarino, A. Oliva, P. Zoccali, M. Camarca, A. Bonanno, and R. A. Baragiola, Phys. Rev. A **50**, 4040 (1994).

[15] S. Mouhammad, P. Benoit-Cattin, C. Benazeth, P. Cafarelli, P. Reynes, M. Richard-Viard, and J. P. Ziesel, J. Phys.: Condens. Matter **10**, 8692 (1998).

[16] L. Guillemot, S. Lacombe, M. Maazouz, E. Sanchez, and V. A. Esaulov, Surf. Sci. **356**, 92 (1996).

[17] L. Guillemot, S. Lacombe, V. N. Tuan, V. A. Esaulov, E. Sanchez, Y. A. Bandurin, A. I. Dashchenko, and V. G. Drobnich, Surf. Sci. **365**, 353 (1996).

[18] M. Guillemot, M. Maazouz, and V. A. Esaulov, J. Phys.: Condens. Matter **8**, 1075 (1996).

[19] S. Lacombe, V. Esaulov, L. Guillemot, O. Grizzi, M. Maazous, N. Mandarino, and V. N. Tuan, J. Phys.: Condens. Matter **7**, L261, (1995).

[20] O. Grizzi, E. A. Sánchez, J. E. Gayone, L. Guillemot, V. A. Esaulov, and R. A. Baragiola, Surf. Sci. **469**, 71 (2000).

[21] M. Barat and W. Lichten, Phys. Rev. A **6**, 211 (1972).

[22] H. S. W. Massey and H. B. Gilbody, in *Electronic and Ionic Impact Phenomena*, Vol. 4 (Clarendon Press, Oxford, 1974).

[23] J. C. Brenot, G. Dhuicq, J. P. Gauyacq, J. Pommier, V. Sidis, M. Barat, and E. Pollack, Phys. Rev. A **11**, 1245 (1975).

[24] J. O. Olson and N. Anderson, J. Phys. B **10**, 101 (1977), see also J. O. Olson *et al.*, Phys. Rev. A **19**, 1457 (1979).

[25] F. Xu, R. A. Baragiola, A. Bonnano, P. Zoccali, M. Camarca, and A. Oliva, Phys. Rev. Lett. **72**, 4041 (1994).

[26] R. Souda, K. Yamamoto, W. Hayami, T. Aizawa, and Y. Ishizawa, Phys. Rev. Lett. **75**, 3552 (1995). See also Surf. Sci. **363**, 139 (1996).

[27] J. W. Rabalais, CRC Crit. Rev. Solid State Mater. Sci. **14**, 319 (1988).

[28] J. W. Rabalais, J. N. Chen, R. Kumar, and M. Narayana, J. Chem. Phys. **12**, 6489 (1985).

[29] O. Grizzi, M. Shi, H. Bu, J. W. Rabalais, and R. A. Baragiola, Phys. Rev. B **41**, 4789 (1990).

[30] O. Grizzi, E. A. Sánchez, S. Lacombe, and V. A. Esaulov, Phys. Rev. B **68**, 085414 (2003).

[31] B. Hird, R. A. Armstrong, and P. Gauthier, Phys. Rev. A **49**, 1107 (1994).

[32] F. Xu, G. Manicò, F. Ascione, A. Bonanno, A. Oliva, and R. A. Baragiola, Phys. Rev. A **57**, 1096 (1998).

[33] F. Ascione, G. Manicò, A. Bonanno, A. Oliva, and F. Xu, Surf. Sci. **394**, L145 (1997). See also *ibid.* **392**, L7 (1996).

[34] K. Wittmaack, Surf. Sci. **345**, 110 (1996).

[35] A. Tolstogouzov, S. Daolio, C. Pagura, and C. L. Greenwood, Surf. Sci. **441**, 213 (1999).

[36] R. Souda, K. Yamamoto, W. Hayami, and T. Aizawa, Surf. Sci. **416**, 320 (1998).

[37] V. A. Esaulov, J. Phys.: Condens. Matter **6**, L699 (1994).

[38] A. L. Boers, Nucl. Instrum. Methods Phys. Res. B **27**, 55 (1987).

[39] R. Souda, T. Aizawa, C. Oshima, and Y. Ishizawa, Nucl. Instrum. Methods Phys. Res. B **45**, 364 (1990).

[40] M. J. Gordon, Rev. Sci. Instrum. **76** (2005).

[41] O. Oen and M. Robinsen, Nucl. Instrum. Methods **132**, 647 (1976).

[42] J. Lindhard and M. Scharff, Phys. Rev. **124**, 128 (1961).

[43] O. B. Firsov, Sov. Phys. JETP **5**, 1192 (1957).

[44] M. Draxler, R. Gruber, H. H. Brongersma, and P. Bauer, Phys. Rev. Lett. **89**, 263201 (2002).

[45] R. Cortenraad, A. W. van der Gon, and H. H. Brongersma, Surf. Interface Anal. **29**, 524 (2000).

[46] W. Eckstein, V. A. Molchanov, and H. Verbeek, Nucl. Instrum. Methods **149**, 599 (1978).

[47] P. Bertrand, Nucl. Instrum. Methods **170**, 489 (1980).

[48] E. C. Goldberg, R. Monreal, F. Flores, H. H. Brongersma, and P. Bauer, Surf. Sci. **440**, L875 (1999). See also R. Cortenraad, A. W. Denier van der Gon, H. H. Brongersma, S. N. Ermolov, and V. G. Glebovsky, Phys. Rev. B **65**, 195414 (2002).

[49] The overall ion survival probability can be expressed as $P^+ = \lfloor P^+_{in}(1-P_{CIN}) + (1-P^+_{in})P_{CIR} \rfloor P^+_{in}$. This result is readily derived by dividing the ion trajectory into three steps where charge exchange may occur: incoming path, hard collision, and outgoing path.

[50] W. Yu, J. L. Sullivan, S. O. Saied, and G. A. C. Jones, Nucl. Instrum. Methods Phys. Res. B **135**, 250 (1998).

[51] A. Tolstogouzov, S. Daolio, and C. Pagura, Nucl. Instrum. Methods Phys. Res. B **217**, 246 (2004).

[52] E. A. García, C. G. Pascual, E. C. Goldberg, J. E. Gayone, E. A. Sánchez, and O. Grizzi, Surf. Sci. **541**, 160 (2003).

[53] J. Slater, in *Quantum Theory of Atomic Structure*, Vol. 1 (McGraw-Hill, New York, 1960), p. 210.

[54] R. Morgensten, A. Niehaus, and G. Zimmermann., J. Phys. B **13**, 4811 (1980).

[55] M. Barat, J. Baudon, M. Abignoli, and J. C. Houver, J. Phys. B **3**, 230 (1970).